LANGMUIR

pubs.acs.org/Langmuir Article

Superior Long-Term Corrosion Inhibition of N80 Steel by New Eco-friendly Hydrazone-Based Compounds in a Simulated Oil Well Acidizing Environment: Establishing the Mechanism at the Molecular Level

Badr El-Haitout, Chaymae Hejjaj, Hassane Lgaz,* Mustafa R. Al-Hadeethi, Omeed Maroof Ali, Han-Seung Lee,* Ismat H. Ali, and Rachid Salghi

Cite This: *Langmuir* 2022, 38, 15937−15949 Read Online

ACCESS | Metrics & More | Article Recommendations | Supporting Information

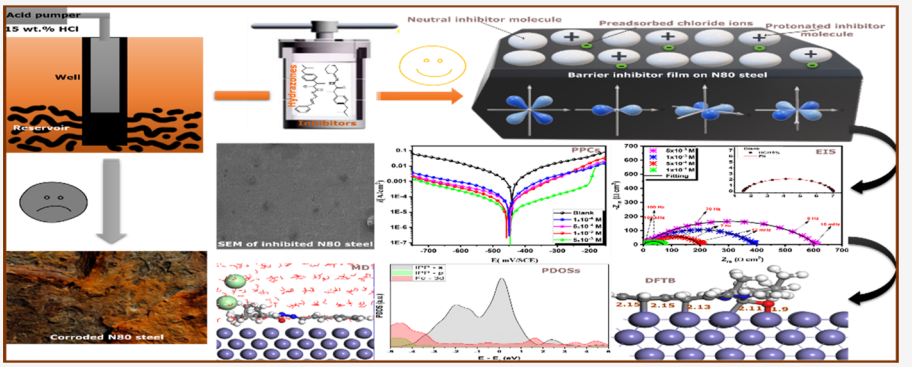

ABSTRACT: The acid treatment process of production wells is one of the most acid-induced corrosive processes. Corrosion inhibitors are an effective tool to inhibit the acids employed in acidizing treatments. Herein, new eco-friendly hydrazone-based compounds, namely, 2-(4-isobutylphenyl)-*N*-((1E,2E)-3-phenylallylidene) propanehydrazide (IPP) and *N*′-cyclohexylidene-2-[4-(2-methylpropyl)phenyl] propanehydrazide (CIP), were prepared through the functionalization of ibuprofen (IBF) and applied for corrosion mitigation of N80 steel in 15 wt % HCl (referred to hereafter as blank). The anticorrosion performance of selected compounds was investigated by employing weight loss (WL), potentiodynamic polarization curves (PPCs), and electrochemical impedance spectroscopy (EIS), complemented by scanning electron microscopy (SEM) and atomic force microscopy (AFM) analyses. In addition, density functional theory-based tight-binding (DFTB) modeling was conducted to get molecular-level insights into inhibitor-metal bonding. Experimental results revealed excellent long-term corrosion inhibition efficiency at very low concentrations of inhibitors and a mixed-type inhibition process. Numerically, N80 steel polarization resistance increased from 5.51 Ω cm^2 in blank to 608.4 and 396 Ω cm^2 in blank inhibited with 5×10^{-3} mol/L of IPP and CIP, respectively, equivalent to 99% and 98% inhibition efficiency based on EIS experiments. Besides, SEM and AFM images showed that, after addition to 15 wt % HCl, inhibitors could effectively prevent the acid attack on the N80 steel surface. The fitting of experimental data to adsorption isotherms indicated that inhibitors' adsorption followed the Langmuir isotherm model and mixed physicochemical adsorption on the metal surface. The DFTB simulation revealed that inhibitor molecules can create covalent and physical interactions with iron atoms, which is further confirmed by partial density of states (PDOSs) analysis.

1. INTRODUCTION

Carbon steel is an extensively used metal in many fields like oil and gas transportation, automotive, and aeronautical sectors because of its desirable chemical, physical, and mechanical properties, availability, and low cost.[1−3] However, despite the high scientific and industrial development achieved in our era, the corrosion of metals and alloys is still the main natural, spontaneous, and destructive phenomenon that causes heavy and sometimes catastrophic losses in industrial or civil infrastructures in terms of economy and safety.[4,5] Hence, high importance has been given to this research field, as demonstrated by so numerous scientific papers and patents published in the last three decades.[6] To overcome this

Received: August 8, 2022
Revised: November 24, 2022
Published: December 13, 2022

https://doi.org/10.1021/acs.langmuir.2c02132
Langmuir 2022, 38, 15937−15949

challenging issue, various protection methods have been suggested and developed to enhance corrosion resistance as well as to reduce the rate of deterioration of metals and alloys. However, the most reported preventive approaches are cathodic/anodic protection, coatings, metal alloying, and corrosion inhibitors.[7]

The protection of metals against corrosion could be done by acting on the solution's state. Inhibitors are widely used because of their low cost, high efficiency, and easy feasibility.[8] Organic compounds with heteroatoms having a single pair of electrons (N, O, and S), aromatic cycles, and aliphatic and conjugate bonds are considered efficient corrosion inhibitors.[9] Nevertheless, many proposed organic corrosion inhibitors are toxic with a low inhibition efficiency for practical applications. In petrochemical processes, to get rid of iron oxide and rust and other no insoluble products, highly concentrated mineral acids such as hydrochloric acid (15−20 wt %)[10,11] are used during acid descaling, oil well acidizing, and acid pickling. This leads to major corrosion issues, especially when acids are injected with low-performance corrosion inhibitors.[12,13] Therefore, there is an urgent need to develop highly efficient and nontoxic compounds to inhibit acid corrosion.

Current efforts in our team are devoted to the development of new corrosion inhibitors with outstanding structural and electronic properties. In this regard, several nonsteroidal anti-inflammatory drugs (NSAIDs) were selected for functionalization as one of the useful synthetic routes. Developed compounds have been tested in various corrosive environments and showed good corrosion inhibition performance.[12,14−16] In continuation of these research efforts, ibuprofen (IBF), which is known by its analgesic and anti-inflammatory activities,[17] is functionalized to synthesize new hydrazone compounds. Despite its wide use, IBF has a poor water solubility that limits its applications. Hence, along with producing efficient corrosion inhibitors through this synthetic route, the functionalization of IBF is also aimed to increase the solubility of the developed hydrazone compounds. On the other hand, hydrazones are well-known for their excellent structural and electronic properties. Their nontoxic nature makes this organic class of compounds a perfect choice for mitigating acid corrosion.[18]

Experimental approaches are widely used to evaluate the anticorrosion properties of organic compounds. This includes several electrochemical, chemical, and surface analytic methods, among others. However, insights into the interactions between the inhibitor molecules and the metal surface at the molecular level are still unreachable from these techniques due to the complexity of the corrosion inhibition process. With the recent major development of hardware and software technologies, computational methods have made it possible to get a deeper insight into the inhibitor−metal interfacial phenomenon.[19,20] First-principles density functional theory (DFT) simulation can be used as to predict the corrosion inhibition mechanisms.[19] However, the implementation of the *ab initio* DFT method can be a very time-consuming process for large adsorption systems. In this regard, the DFT-based tight-binding (DFTB) method, which is as accurate as the *ab initio* DFT method and much faster than it, can be an excellent alternative for simulating large systems.[12,21,22] In contrast to quantum chemical parameters derived from fitted DFT calculations, DFTB can provide insights into the charge transfer and bonding characteristics between adsorbed molecules and the metal surface, facilitating a more comprehensive description of the corrosion inhibition mechanism. However, when considering the adsorption of organic molecules on metal surfaces, solid/water is the more relevant interface as the adsorption is competitive, and several competing effects such as water−surface, molecule−water, and molecule−surface affect the adsorption energy.[23,24] Also, in real conditions, the metal surface is not clean and contains many chemical species such as solvent molecules while the solid/vacuum interface represents a clean metal surface.[25] Herein, the simulation results refer to the solid/vacuum interface for purely modeling reasons. Even so, another vital point to keep in mind is the significant gaps in time and length scales in the simulations relative to the experiments. Hence, the presented results should be taken cautiously. The main focus of the simulation section of the present work is to get initial insights into the chemistry of inhibitor−molecule−metal bonding and not intended for direct correlation with experimental findings.

Furthermore, several reports highlighted the very limited contribution of quantum chemical parameters and molecular dynamics simulation to understanding the corrosion inhibition process.[26] Quantum chemical parameters provide basic information about the reactivity of inhibitor molecules without considering the metal surface and solvent, thus giving little physical insights, while classical molecular dynamics cannot describe bond formation/breaking except in the case of reactive force fields.[26,27] Given these limitations, in the present work, a specific focus will be given to DFTB simulations while other theoretical calculations will be reported as Supporting Information.

Considering the above-mentioned facts, we report herein the corrosion inhibition properties and adsorption characteristics of two hydrazone derivatives derived from ibuprofen, namely 2-(4-isobutylphenyl)-*N*-((1*E*,2*E*)-3-phenylallylidene) propanehydrazide (IPP), and *N*′-cyclohexylidene-2-[4-(2-methylpropyl)phenyl] propanehydrazide (CIP) for N80 steel corrosion in 15 wt % HCl solution. Weight loss measurements, potentiodynamic polarization and electrochemical impedance spectroscopy were performed to evaluate the corrosion inhibition performance of investigated hydrazones. The surface morphology of the N80 steel was analyzed using a scanning electron microscopy (SEM) and atomic force microscopy (AFM). In addition, comprehensive DFTB simulations were conducted to investigate the adsorption characteristics of studied molecules on the steel surface, aiming to propose a more accurate description of the corrosion inhibition mechanism.

2. MATERIALS AND METHODS

2.1. Synthesis of Compounds, Materials, and Solutions. Chemical and electrochemical experiments were performed using N80 steel having the following composition (in wt %): 0.31% C, 0.19% Si, 0.92% Mn, 0.01% P, 0.008% S, 0.2% Cr, and balance Fe. N80 steel samples were cut into 2.5 cm × 2 cm × 0.025 cm and 5 cm × 0.7 cm × 0.3 cm for weight loss and electrochemical tests. Details about sample preparation and chemicals have been reported in our recent work.[28] The investigated compounds were prepared according to the procedure reported in the Supporting Information, and a concentration range of 1×10^{-4} - 5×10^{-3} mol/L was used in all experiments after several pretrial tests.

2.2. Gravimetric Measurements. The gravimetric method is a very fundamental corrosion measurement technique. Weight loss tests were carried out for N80 steel samples immersed in blank and inhibited solutions using various concentrations of IPP and CIP

https://doi.org/10.1021/acs.langmuir.2c02132
Langmuir 2022, 38, 15937−15949

compounds at 303 K. To ensure the reproducibility of results, weight loss tests were repeated three times with ±5−7% difference between tests. More details about weight loss tests and experiment standards can be found in our previous work[28] and ASTM standard.[29] The corrosion rate (C_R) inhibition efficiency ($\eta_{WL}(\%)$), and surface coverage (θ) were used to evaluate the effect of tested compounds on the corrosion of N80 steel in 15 wt % HCl by applying the following eqs 1−3:

$$C_R = \frac{K \times \Delta m}{A \times t \times \rho} \quad (1)$$

$$\eta_{WL}(\%) = \frac{C_{R^\circ} - C_{R^i}}{C_{R^\circ}} \times 100 \quad (2)$$

$$\theta = \frac{C_{R^\circ} - C_{R^i}}{C_{R^\circ}} \quad (3)$$

In eq 1, K and ρ are constant ($K = 8.76 \times 10^4$, $\rho = 7.86$ g/cm^3), while t, A, and Δm represents the immersion time, the steel surface area, and the weight loss of the steel samples at time t. In eqs 2 and 3, C_{R° and C_{R^i} denote the corrosion rate without and with different inhibitor concentrations, respectively.

2.3. Electrochemical Measurements. A classical three-electrode system connected to a Corrtest potentiostat/galvanostat model CS350 was used to perform all electrochemical measurements. The N80 steel was used as a working electrode, while a saturated calomel electrode (SCE) and platinum wire were used as a reference electrode and counter-electrode (CE). An open circuit potential (OCP) test was launched 0.5 h before every electrochemical experiment to reach the steady state condition. All EIS measurements were performed by applying an alternating current with an amplitude of 5 mV in the frequency range of 100 kHz to 100 mHz. The EIS data were fitted and simulated to the appropriate equivalent circuits using EC-Lab software. PPCs were determined in a corrosion potential range of ±250 mV from open circuit potential (OCP) at a scan rate of 1.0 mV/s. The polarization resistance R_p and corrosion current densities i_{corr} values obtained from EIS and PPCs tests were used to determine the inhibition efficiency using eqs 4 and 5, respectively:

$$\eta_{EIS}(\%) = \frac{R_p^i - R_p^\circ}{R_p^i} \times 100 \quad (4)$$

$$\eta_{PDP}(\%) = \frac{i_{corr}^\circ - i_{corr}}{i_{corr}^\circ} \times 100 \quad (5)$$

where R_p°, i_{corr}° and R_p^i, i_{corr} denote the polarization resistance and corrosion current density values without and with concentration of inhibitors, respectively.

2.4. SEM and AFM Analyses. The N80 steel morphology and its roughness roughness/smoothness were evaluated through SEM and AFM after 24 h immersion in blank and HCL solutions inhibited with 5×10^{-3} mol/L of inhibitor at 303 K. The N80 steel samples were prepared following the same procedure described in section 2.1, then analyzed using a field emission scanning electron microscope (FE-SEM, MIRA3 model, TESCAN, Czech Republic) operated at 15 kV. The surface topography and roughness of the corroded and inhibited samples was evaluated using AFM (Park XE-100: Atomic Force Microscopy, Suwon, South Korea) at 10 cm × 10 cm and 5 cm × 5 cm scan ranges for uninhibited and inhibited samples in a contact mode. AFM image processing was conducted using Gwyddion modular software.

2.5. Theoretical Calculations. *2.5.1. Quantum Chemical Parameters.* DFT calculations were applied to provide useful information into structural and electronic properties of investigated compounds and reveal where the active donor/acceptor sites are located. Global and local reactivity descriptors were generated using the Generalized Gradient Approximation (GGA) functionality with PBE parametrization and double numerical basis sets plus polarization (DNP) using Dmol3 code[30] implemented in Materials Studio software. The aqueous phase was modeled using the COSMO solvation model.[31] All geometry optimization parameters were equivalent to "fine" quality in Dmol3 code.

2.5.2. DFTB Simulations. Interactions between inhibitor molecules and the iron surface surface were investigated at molecular level using spin-polarized self-consistent charge DFTB (SCC-DFTB) calculations. The trans3d Slater−Koster parameters were implemented to describe the interaction between inhibitor molecules and the iron surface. Besides, an empirical dispersion correction was applied. To speed up the convergence, 0.01 smearing, SCC tolerance set to 10^{-8}, and Broyden mixing scheme were used. Other convergence thresholds were equivalent to "fine" quality in the DFTB+ code. Details about simulation cell construction and DFTB optimization are available in our recent work.[28] All calculation were performed using the DFTB+ software.[32] The interaction energy (E_{inter}) was calculated to evaluate the interaction strength of compounds with the iron surface using the equation bellow:

$$E_{inter} = E_{Mol/surf} - (E_{surf} + E_{Mol}) \quad (6)$$

where $E_{Mol/surf}$, E_{surf}, and E_{Mol} refer to the total energy values of inhibitor-Fe(110), the Fe(110) slab, the isolated molecule, respectively.

2.5.3. Molecular Dynamics Simulations. The most stable adsorption configurations of a single molecule of IPP and CIP compounds on the surface of Fe(110) were studied by MD simulation using the Forcite module of Materials Studio. To this end, the unit cell of Fe, exported from the database of Material studio software, was cleaved at the surface (110) and replicated 5 times in the x- and y-directions to obtain a supercell. To reduce the effect of periodic replicas, a space of 30 Å was inserted at the z-axis of the created supercell. After adding 1680 water molecules, 10 Cl^-, 10 H_3O^+, and the optimized inhibitor molecules into the supercell, the adsorption system was geometrically optimized according to the Smart algorithm. Molecular dynamics simulation was carried out under the NVT ensemble (canonical, i.e., the number of particles N, the volume V, and the temperature T of the system were kept constant), 303 K, 1 fs time step, and 5000 ps simulation time. The COMPASS force field was used in the whole process.[33] Other simulation parameters were equivalent to "fine" quality in the Forcite module.

3. RESULTS AND DISCUSSION

3.1. Gravimetric Measurements. Gravimetric tests for N80 steel samples in 15 wt % HCl without and with various inhibitor concentrations were performed after 24 h immersion period at 303 K, and the resultant parameters are shown in Table 1 and Figure S1 (Supporting Information). Weight loss tests can provide general information on the dissolution of steel samples in blank and inhibited solutions. Although it is a simple measurement, it can help estimate the speed of metal

Table 1. Effect of IPP and CIP Concentrations on the Corrosion Rate of N80 Steel in 15 wt % HCl Solution at 303 K

[inhibitor] (mol/L)	W (mm/y)	Θ	η_{WL} (%)
blank	22 ± 0.024		
IPP			
5×10^{-3}	0.880 ± 0.057	0.96	96.00
1×10^{-3}	1.100 ± 0.078	0.95	95.00
5×10^{-4}	1.430 ± 0.043	0.93	93.50
1×10^{-4}	2.420 ± 0.064	0.89	89.00
CIP			
5×10^{-3}	1.100 ± 0.056	0.95	95.00
1×10^{-3}	1.364 ± 0.089	0.93	93.80
5×10^{-4}	1.760 ± 0.063	0.92	92.00
1×10^{-4}	2.860 ± 0.022	0.87	87.00

https://doi.org/10.1021/acs.langmuir.2c02132
Langmuir 2022, 38, 15937−15949

degradation. The corrosion rate calculated from weight loss tests is substantially decreased after adding inhibitors to 15 wt % HCl. It goes from 22 mm/year for the blank solution to 0.88 and 1.1 mm/year in the inhibited solutions with IPP and CIP inhibitors, respectively. An increased dosage of inhibitors leads to a very low corrosion rate compared to a blank sample, signifying that added inhibitors create a barrier against acid corrosion.

Consequently, the corrosion inhibition efficiency follows the same trend; a higher concentration of inhibitors leads to an increased inhibition efficiency value. This effect is mainly associated with a change in the steel/electrolyte interface due to inhibitor molecules' adsorption on the steel surface and the repletion of water molecules. This assumption can further be confirmed and explained by electrochemical results.

Reviewing literature from previous researchers shows that several compounds were reported as corrosion inhibitors for steel in 15 wt % HCl. Some of the recent organic compounds used as corrosion inhibitors for steel in 15 wt % HCl are listed in Table S1 (Supporting Information) with their experimental conditions. Despite the differences in experimental conditions, it can be observed that all listed inhibitors exhibit good anticorrosion properties. The IPP and CIP hydrazones show good inhibiting performance toward the N80 steel corrosion in the simulated corrosive medium at 303 K, which stemmed from their electron-rich molecular structures that contain several heteroatoms and functional groups able to act as adsorption sites when interacting with the N80 steel surface.

3.2. Potentiodynamic Polarization Tests. The corrosion kinetics of anodic and cathodic reactions of N80 steel in 15 wt. % HCl without and with various inhibitor concentrations at 303 K are evaluated by potentiodynamic polarization curves. The results are shown in Figure 1. Electrochemical kinetic parameters such as corrosion potential (E_{corr}), corrosion current density (i_{corr}), anodic and cathodic Tafel slopes (βa, βc) determined by Tafel extrapolation of linear segments of PPCs are tabulated in Table 2 along with inhibition efficiency values.

A visual analysis of results in Figure 1 shows a significant decrease in anodic and cathodic current densities after adding different hydrazones concentrations to 15 wt.% HCl solution. The PPCs shape remains almost unchanged in the cathodic domain after adding inhibitors to the acid solution while a substantial decrease of current density is noticed. This behavior at cathodic potential suggests that inhibitors do not affect the cathodic reaction mechanism (hydrogen evolution).[34] A similar remark can be drawn for anodic branches of PPCs, which also decrease up to −300 to −200 mV/SCE, from which the PPCs suddenly increased, especially for 5×10^{-3} mol/L of inhibitors. However, even at more anodic potentials, inhibitors still remarkably affect the anodic corrosion reaction. Such behavior is mainly attributed to the desorption of adsorbed molecules at more positive potentials, usually called desorption potential.[10] The remarkable shift in current densities toward lower values is accompanied by almost no changes in the corrosion potentials, suggesting that both inhibitors simultaneously decrease the kinetic of anodic and cathodic N80 steel corrosion reactions by exerting a mixed inhibition effect.

The data analysis in Table 2 confirms the decrease in corrosion current density (i_{corr}) values in the presence of inhibitors. For instance, i_{corr} values reach 51 μA cm^{-2} for IPP, and 68 μA cm^{-2} for CIP compared to a blank (1711 μA cm^{-2}),

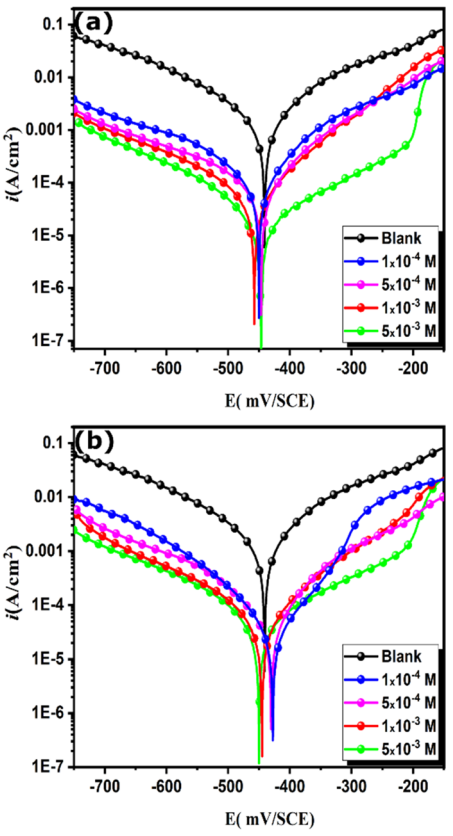

Figure 1. Potentiodynamic polarization curves of N80 steel determined from blank and inhibited 15 wt % HCl solutions at 303 K: (a) IPP and (b) CIP.

signifying the high inhibition effect of inhibitors on the steel corrosion process. In addition, results reveal no significant changes in anodic and cathodic Tafel slopes and a slight displacement of 17 mV/SCE in corrosion potentials toward the cathodic domain. It is well-reported that a long-range corrosion potential displacement of the order of 80 mV in anodic or cathodic directions indicates an anodic or cathodic characteristic of the tested compound.[35−37] From data in Figure 1 and Table 2, we can notice a slight shift of corrosion potential values to the cathodic direction, except 10^{-4} and 5×10^{-4} mol/L of CIP. This small corrosion potential displacement indicates that, at higher concentrations, investigated compounds tend to block the cathodic corrosion reaction more than the anodic one. However, given the very small shift of corrosion potential values, tested compounds are far from being classified as cathodic corrosion inhibitors. Therefore, their mixed-type characteristic is well-confirmed.

A concentration-dependence effect is observed for both inhibitors in terms of inhibition performance. The inhibition efficiency increases by increasing the inhibitor dosage and reaches a maximum of 97% and 96% for IPP and CIP, respectively. However, both inhibitors show excellent inhibition performance at all studied concentrations. For instance, at a low concentration of 10^{-4} mol/L, IPP and CIP keep good performance of 90% and 89%, respectively.

3.3. EIS Measurements. The EIS plots in Nyquist and Bode forms for N80 steel corrosion are determined without and with various inhibitor concentrations at 303 K temperature. As illustrated in Figure 2a and b, Nyquist diagrams show a single capacitive loop and an increased diameter of the

https://doi.org/10.1021/acs.langmuir.2c02132
Langmuir 2022, 38, 15937−15949

Table 2. Electrochemical Parameters of N80 steel in 15 wt % HCl without and with Various Concentrations of IPP and CIP and Corresponding Inhibition Efficiency Values at 303 K

[inhibitor] (mol/L)	$-E_{corr}$(mV vs SCE)[a]	$-\beta_c$(mV dec^{-1})[b]	β_a(mV dec^{-1})[c]	i_{corr}(μA cm^{-2})[d]	η_{PDP} (%)
blank	440	111	90	1711	
IPP					
5×10^{-3}	446	96	103	51	97.01
1×10^{-3}	457	107	105	68	96.02
5×10^{-4}	447	98	102	90	94.73
1×10^{-4}	450	109	145	171	90.00
CIP					
5×10^{-3}	449	91	104	68	96.02
1×10^{-3}	445	113	106	86	94.97
5×10^{-4}	430	97	100	103	93.98
1×10^{-4}	427	115	108	188	89.01

[a]The standard deviation range for E_{corr}: [3.1−6.3%]. [b]The standard deviation range for β_c: [5.2−7.5%]. [c]The standard deviation range for β_a: [3.7−6.2%]. [d]The standard deviation range for i_{corr}: [4.7−7.9%].

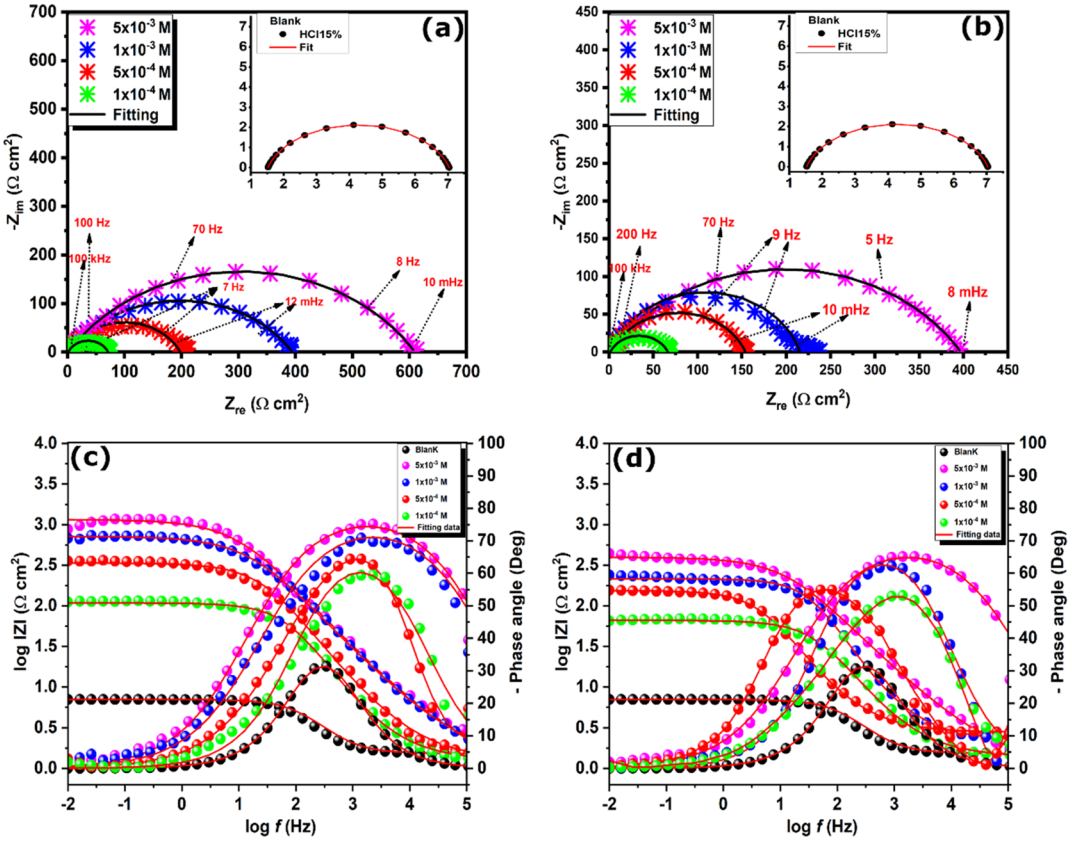

Figure 2. Nyquist and Bode diagrams of N80 steel in 15 wt % HCl with and without various concentrations of inhibitors: (a, c) IPP and (b, d) ICP.

capacitive half loops with increasing inhibitor concentration. It signifies that inhibitors' performance is a function of their concentration and that a charge transfer mechanism controls the corrosion and corrosion inhibition processes. The significant increase in diameter of the capacitive half loops after adding an increasing amount of inhibitors is mainly due to the formation of a barrier film on the N80 steel surface, thus limiting the charge transfer.[38] In addition, the spectra show half loops with a depressed center below the real axis as an indicator of the heterogeneous nature of the electrode surface.[39−41] The Bode phase angle plots vs frequency are shown in Figure 2c and d. As shown in the figure, Bode diagrams display only one time constant at all concentrations, suggesting only one relaxation process and increased phase angle values with the increase of inhibitor concentration. The inhibitors' adsorption can also be confirmed by the noticeable broadening at the intermediate frequencies. Besides, given the fact that all maximum phase angle values are lower than the maximum possible phase shift, i.e., −90°,[42] results confirm the nonideal behavior attributed to the heterogeneous nature of the steel surface.[39−41] It has been reported that the phase angle values at higher frequencies can be correlated with the corrosion protection performance.[43,44] From results in Figure 2c and d, we notice that the phase angle values at 3 kHz increase with increasing inhibitor concentration, suggesting an increased corrosion inhibition performance.

Figure S2 shows the equivalent electrical circuit (EEC) used to fit experimental EIS results. An excellent parametric fit of

https://doi.org/10.1021/acs.langmuir.2c02132
Langmuir 2022, 38, 15937−15949

Table 3. EIS Parameters for N80 Steel in Blank and 15 wt % HCl Inhibited with Different Concentrations of IPP and CIP at 303 K

[inhibitor] (mol/L)	R_p(Ω cm^2)[a]	n[b]	Q ($\mu\Omega^{-1}$ s^n cm^{-2})[c]	R_s(Ω cm^2)[d]	$C_{eff\,dl}$(μF cm^{-2})	η_{EIS} (%)
blank	5.51 ± 1.3	0.837 ± 0.004	697.8 ± 1.353	1.50	174	
IPP						
5×10^{-3}	608.4 ± 1.5	0.836 ± 0.003	182 ± 2.045	1.22	34	99.09
1×10^{-3}	393.6 ± 1.7	0.830 ± 0.001	223 ± 1.643	1.17	41	98.60
5×10^{-4}	196.6 ± 1.6	0.812 ± 0.009	387 ± 1.712	1.25	65	97.20
1×10^{-4}	69.75 ± 1.2	0.856 ± 0.005	491 ± 1.234	1.24	140	92.11
CIP						
5×10^{-3}	396 ± 0.4	0.845 ± 0.005	231 ± 1.546	1.08	50	98.61
1×10^{-3}	213.1 ± 1.6	0.817 ± 0.004	314 ± 0.673	2.26	61	97.41
5×10^{-4}	151.1 ± 1.3	0.839 ± 0.007	405 ± 0.534	2.79	109	96.36
1×10^{-4}	65.05 ± 0.8	0.849 ± 0.008	513 ± 1.564	1.40	141	91.54

[a]The standard deviation range for R_p: [6.7−7.1%]. [b]The standard deviation range for n: [4.3−8.2%]. [c]The standard deviation range for Q: [5.7−8.3%]. [d]The standard deviation range for R_s: [4.6−7.9%].

the experimental impedance spectra for all concentrations is achieved using this EEC. In the equivalent circuit in Figure S2, R_s refers to the solution resistance, R_p is the polarization resistance, CPE(Q, n) is the constant phase element, with Q denoting the CPE constant and n being the heterogeneity measure. Table 3 regroups all parameters derived from EIS tests along with the calculated inhibition efficiency of all concentrations. In the EEC, the CPE has been used to model the nonideal capacitor. The relationship between the CPE and the impedance is represented by the following eq 7.

$$Z_{CPE} = \frac{1}{Q(j\omega)^n} \tag{7}$$

where j and ω denote the imaginary number and the angular frequency, respectively.

The Brug equation[45] was used to calculate the effective capacity $C_{eff\,dl}$:

$$C_{efff,dl} = Q_{dl}^{1/n} \times \left(\frac{1}{R_s} + \frac{1}{R_p}\right)^{n-1/n} \tag{8}$$

The inhibitors' performance is estimated numerically by determining the corrosion inhibition efficiency using polarization resistance, which is the sum of all resistances at the steel/electrolyte interface. Hence, parameters obtained from fitting EIS data and inhibition efficiency values are determined and reported in Table 3.

From Table 3, the values of R_p are increased with an increase in the concentration of IPP and ICP and are larger than blank. For IPP, the R_p reaches a value of 608.4 Ω cm^2, while that of CIP increase to 396 Ω cm^2 compared to the blank test, which is associated with a very low polarization resistance of 5.51 Ω cm^2. Besides, it can be observed that the $C_{eff\,dl}$ values significantly decreased after the addition of increasing dosage of inhibitors. It has been stated that "*the significant decrease in the capacitance values can be attributed to an increase in the thickness of the double electric layer due to the inhibitor's adsorption on the metal surface*".[28,46] In this situation, the adsorption of inhibitor molecules leads to the modification of the double layer behavior due to the inhibitor film formed on the steel surface.[47,48] That is said, the strength of adsorption is associated with inhibitors' molecular structures and the stable adsorption geometry over the steel surface. Deep insights about this will be given in theoretical sections. The inhibition efficiency calculated from EIS shows an increasing trend similar to that obtained from PPCs. The inhibition efficiency of investigated compounds reaches a high value of 99% and 98% for IPP and CIP, respectively. In addition, inhibitors have a strong inhibition effect on acid corrosion of N80 steel at very low concentrations, i.e., an inhibition efficiency higher than 90% at 10^{-4} mol/L.

On the other hand, the corrosion inhibition performance of investigated inhibitors is evaluated at longer immersion times to examine the stability of the adsorbed inhibitor layer. To this end, EIS experiments were performed for steel in 15 wt % HCl at different immersion times (1−24 h), in the presence of 5×10^{-3} mol/L of IPP inhibitor. Experiments were limited to 24 h given the fact that it is enough time to protect tubings against corrosion. Hence, useful information about tested compound's ability to protect N80 steel can be obtained. Figure S3 (Supporting Information) represents Nyquist plots of N80 steel in 15 wt % HCl inhibited with 5×10^{-3} mol/L IPP at different immersion times.

The radius of depressed semicircles in the Nyquist curves increased at early immersion periods (1 and 6 h), reaching its maximum at 12 h with a value of 700 Ω cm^2. The polarization resistance values, starting with a value of 608.4 (Ω cm^2) in the first hour of immersion and decreased to a value of 451.3 Ω cm^2 after 24 h. The results show that the inhibition effect reaches its maximum at 12 h and then starts decreasing. At the early immersion stage, inhibitor molecules adsorb on the N80 steel surface, creating a multilayer of inhibitor molecules covering a wide surface area. However, an increased amount of inhibitor molecules will increase their density, favoring the desorption of molecules from the steel surface because of van der Waals force between adsorbed molecules. In this situation, the created inhibitor layer loses its stability.[46] With this said, the investigated inhibitor still keeps high corrosion protection of N80 steel at 24 h. This may be explained by the strong bonding between inhibitor molecules and vacant iron d-orbitals.

3.4. Adsorption Isotherm. Adsorption isotherms are one of the essential tools for getting insights into the adsorption mode of inhibitor molecules on the metal surface. In the present work, it is well-confirmed from electrochemical impedance results that the addition of inhibitor molecules to 15 wt % HCl decreases the effective double layer because of the increased thickness of formed inhibitor film as a result of inhibitor adsorption. Therefore, several adsorption isotherms are fitted to experimental data from weight loss methods to

https://doi.org/10.1021/acs.langmuir.2c02132
Langmuir 2022, 38, 15937−15949

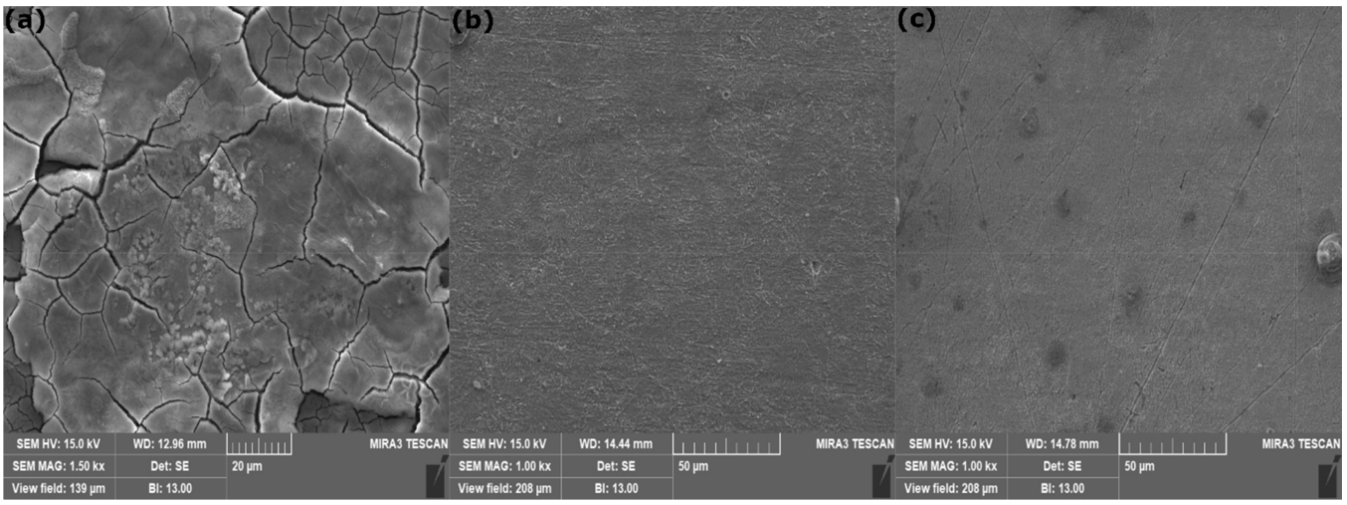

Figure 3. FE-SEM analysis of N80 steel immersed in blank (a) and HCl solutions inhibited with IPP (b) and CIP (c) after 24 immersion time.

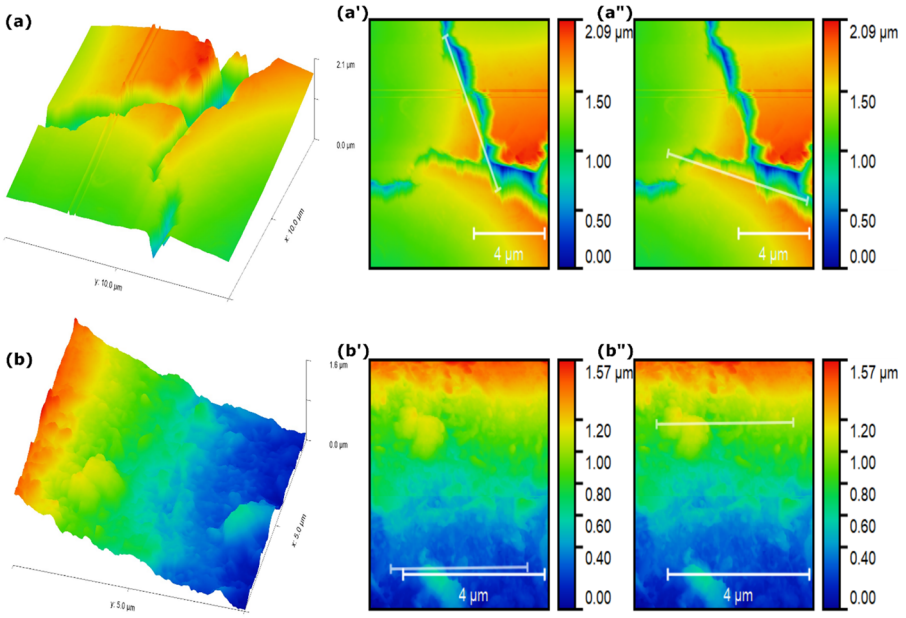

Figure 4. AFM topographical analysis of N80 steel immersed in blank (a) and HCl solution inhibited with IPP (b) after 24 immersion time. (a',a") and (b',b") represent the 2D images.

determine the most suitable adsorption isotherm model. However, among tested isotherms, the model of Langmuir was found more appropriate for the description of the adsorption process of hydrazones on N80 steel surface. The linear relationships of C_{inh}/θ vs C_{inh} (C_{inh}: inhibitor concentration) representing the Langmuir isotherm is shown in Figure S4 (Supporting Information). The Langmuir adsorption isotherm is expressed by the following eq 9:

$$\frac{C_{inh}}{\theta} = \frac{1}{K_{ads}} + C_{inh} \tag{9}$$

where θ is the surface coverage obtained from weight loss measurements and K_{ads} is the adsorption equilibrium constant.

The plot in Figure S4 (Supporting Information) is a straight line with a correlation coefficient (R^2), and slope values are close to 1 for IPP and CIP inhibitors, as indicated in Table S2 (Supporting Information). The Langmuir constant K_{ads} value is calculated from Figure S4 based on the intercept of the straight lines of C_{inh}/θ versus C_{inh}; its relationship with ΔG_{ads} is given by the following eq 10:

$$\Delta G^{\circ}_{ads} = -RT \ln(K_{ads} \times 55.5) \tag{10}$$

where R is the universal gas constant (8.314 J K^{-1} mol^{-1}) and T is the absolute temperature (303 K); 55.5 represents the numerical equivalent of the molar concentration of H_2O in mol/L. The calculated values of K_{ads} and ΔG_{ads} are given in Table S2 (Supporting Information).

The Langmuir isotherm model is based on the following assumptions: inhibitor molecules are adsorbed on well-defined sites of the steel surface in an identical way and independently of the adjacent sites. It means a homogeneous surface without congestion between adsorbed molecules. Looking at the results in Table S2 (Supporting Information), one can notice large negative values of the standard free energy, suggesting that inhibitor molecules absorb by an appreciable extent on the N80 steel surface. On the other hand, according to previous

https://doi.org/10.1021/acs.langmuir.2c02132
Langmuir 2022, 38, 15937−15949

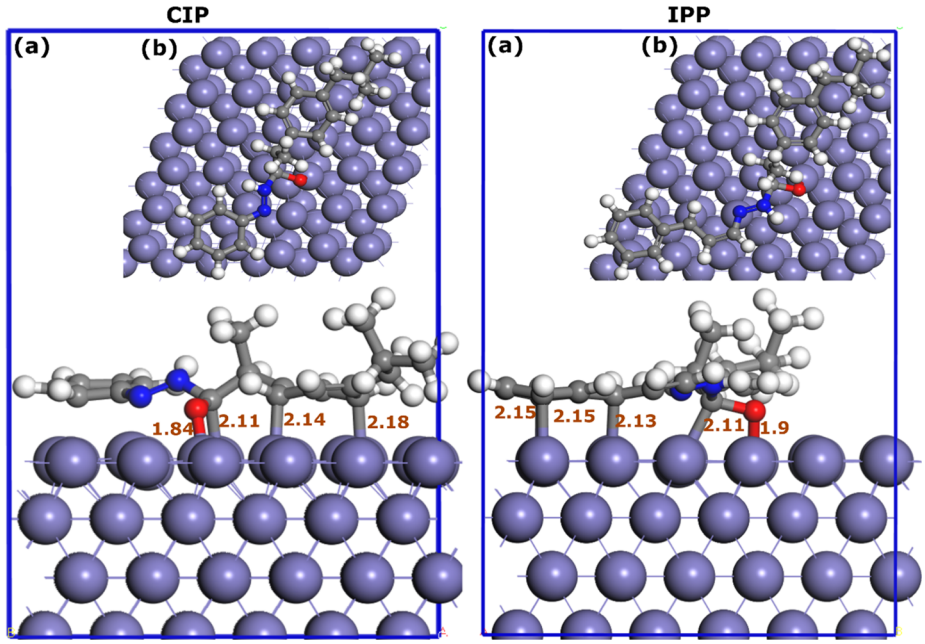

Figure 5. Optimized adsorption geometries of IPP and CIP molecules on the Fe(110) surface obtained via DFTB calculations: (a) side view and (b) top view. All optimized bond lengths are in Å.

works,[49−51] the type of adsorption can be predicted from the ΔG_{ads} value as follows: The inhibition mechanism is classified as physisorption if the ΔG_{ads} value is up to −20 kJ/mol. However, a ΔG_{ads} value more negative than −40 kJ/mol is an indicator of chemical adsorption. The calculated values of ΔG_{ads} range from −20 to −40 kJ/mol, which is typically classified as a mixed adsorption process; i.e., the inhibition action is a physicochemical adsorption process.[52,53]

Heteroatoms of hydrazone inhibitor molecules can immediately get protonated in a strong acidic medium. Bearing in mind that chloride ions are quickly adsorbed on the N80 steel surface, physical interactions would be the first step that promotes the adsorption of inhibitor molecules on the metal surface. When inhibitor molecules approach the metal surface, there will be high chances for chemical interactions between molecules' active sites such as heteroatoms and aromatic rings and vacant d orbitals of iron atoms. Also, when strong charge transfer from molecules to steel surface occurs, electron-back-donation from steel surface to empty π^* of inhibitor molecules would remove the excess of electron density. This will make the adsorption of inhibitor molecules stronger and more stable. The theoretical sections will discuss more details about the corrosion protection mechanism.

3.5. SEM Analysis. SEM analysis is a valuable surface characterization technique to evaluate the morphological changes observed before and after adding inhibitors for 24 h in 15 wt % HCl solution. Figure 3 shows SEM images of N80 steel in its corroded and inhibited conditions. Without hydrazone inhibitors, i.e., in the blank test (Figure 3a), a highly damaged steel surface morphology can be observed with several unstructured corrosion products. However, the N80 steel surface becomes smooth without severe corrosion attack after the addition of 5×10^{-3} mol/L of inhibitors. These morphological changes are due to the effective adsorption of inhibitor molecules on the N80 steel surface, creating a barrier against corrosion attack.

3.6. AFM Topographical Analysis. The corrosion protection performance of the compounds in this study is further investigated using atomic force microscopy. The total roughness of the whole scan area of the corroded and inhibited N80 steel surface can provide helpful information about the effect of the inhibitor's addition to HCl solution on the surface morphology of N80 steel. The 3D and 2D AFM surface topographies of N80 steel immersed in 15 wt % HCl without and with 5×10^{-3} mol/L IPP are shown in Figure 4. In addition, 2D images show the line scans for measuring the surface roughness of samples in two different areas. It is observed that corroded N80 steel exhibits an irregular and rough surface consistent with SEM images of corroded N80 steel. The absolute roughness value (R_a) of N80 steel in 15 wt % HCl is 131 nm. However, the surface of N80 steel immersed in 15 wt % HCl with an optimum inhibitor concentration can be considered macroscopically flat, with R_a decreasing to 53 nm, compared to values of the blank test. The same can be said about parameters derived from line scans of specific parts of corroded and inhibited N80 steel samples. For the blank test, R_a values are 61.93 and 35.69 nm for Figure 4a' and a", respectively, which decrease to 14.47 and 16.89 nm for Figure 4b' and b", respectively, after the addition of inhibitor to the 15 wt % HCl. These morphological differences confirm that the inhibitor significantly decreases the corrosivity of the HCl solution by forming a protective inhibitor layer limiting the acid attack.

3.7. Density-Functional Based Tight Binding (DFTB). *3.7.1. Energetic and Geometries.* Experimental studies of corrosion inhibition are fundamental for estimating the performance of investigated corrosion inhibitors and the mechanism by which the inhibition is achieved. However, it is hard to get many aspects of the adsorption process from experiments. That is why theoretical simulations are frequently used to understand better the adsorption geometries of studied inhibitors and other physical insights that are not available from the experiment.[20,54] Bearing this in mind, the present

https://doi.org/10.1021/acs.langmuir.2c02132
Langmuir 2022, 38, 15937−15949

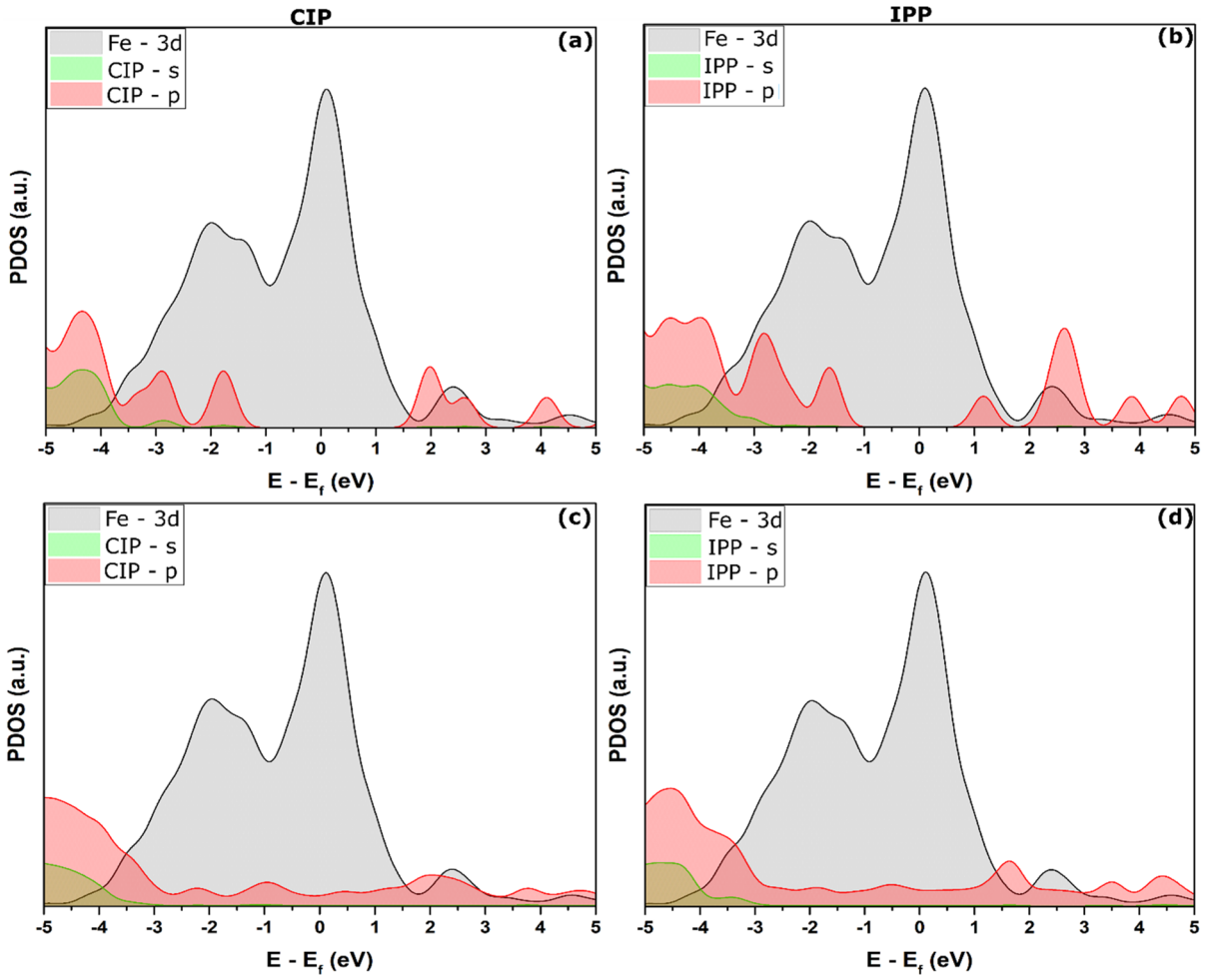

Figure 6. Projected density of states of inhibitor-Fe(110) adsorption systems: (a, b) PDOS of isolated molecules and (c, d) PDOS of adsorbed inhibitor molecules on the Fe(110) surface.

section reports the theoretical simulation results of the interactions between investigated inhibitor molecules and Fe(110) surface. Snapshots of the most stable adsorption geometries of the studied inhibitors over the Fe(110) surface obtained by DFTB simulations are shown in Figure 5. A visual inspection reveals that both inhibitor molecules adsorb on the iron surface in a near parallel disposition, the most frequent adsorption mode of large organic molecules on metal surfaces.[21]

After geometric optimization, the IPP molecule forms several covalent bonds with iron atoms with distance lengths between 1.90 and 2.15 Å. Several bonds are formed between IPP's carbon atoms and iron surface. The nature of the bonding can be classified from the sum of covalent radii for Fe−C. It is known that the sum of the covalent radii for Fe−C is $r_C + r_{Fe}$ = 2.08 Å.[55] The Fe−C distances range between 2.1 and 2.15 Å, suggesting that chemical bonds are formed between IPP's carbons and Fe atoms. In addition, the oxygen atom of the carbonyl group also has a covalent interaction with the iron surface, as indicated by the Fe−O distance (1.90 Å) that is within the sum of covalent radii for Fe−O ($r_O + r_{Fe}$ = 1.98 Å).[55] On the other hand, it should be noted that the ibuprofen moiety of the IPP molecule has no chemical interactions with Fe atoms.

In the case of the CIP molecule, like the IPP molecule, atoms of the carbonyl group are also bonded to the Fe surface with bonding distances lie in between 1.84 and 2.18 Å, which is close to the sum of their covalent radii ($r_O + r_{Fe}$ = 1.98 Å and $r_C + r_{Fe}$ = 2.08 Å).[55] Besides, carbon atoms of the ibuprofen moiety form two Fe−C bonds with distances between 2.11 and 2.18 Å, which also fall within sum of their covalent radii, thus implying covalent interactions. Unlike carbon and oxygen atoms, nitrogen atoms of both molecules do not form any bond with the iron surface. The Fe−N bond distances are within 3 Å; it leads us to guess that nitrogen atoms might physically interact with the iron surface. Such interactions are highly possible due to the strong affinity of nitrogen atoms to protonation.

In terms of interacting energies, IPP and CIP have interaction energies of −1.33 and −1.19 eV, respectively. Both adsorption systems' strong negative interaction energies might also involve the contribution of physical interactions. Besides, the IPP molecule has a higher interaction energy than that of CIP, mainly due to the higher contribution of π-molecular orbitals.[56] This is obvious from the several covalent bonds formed between the IPP molecules and Fe surface compared to only four covalent bonds between CIP molecules and iron atoms.

3.7.2. Projected Density of States. The geometrical optimization of the inhibitor-Fe(110) adsorption systems shows that inhibitor molecules can form covalent bonds with iron atoms. However, further investigation and analysis of the

https://doi.org/10.1021/acs.langmuir.2c02132
Langmuir 2022, 38, 15937−15949

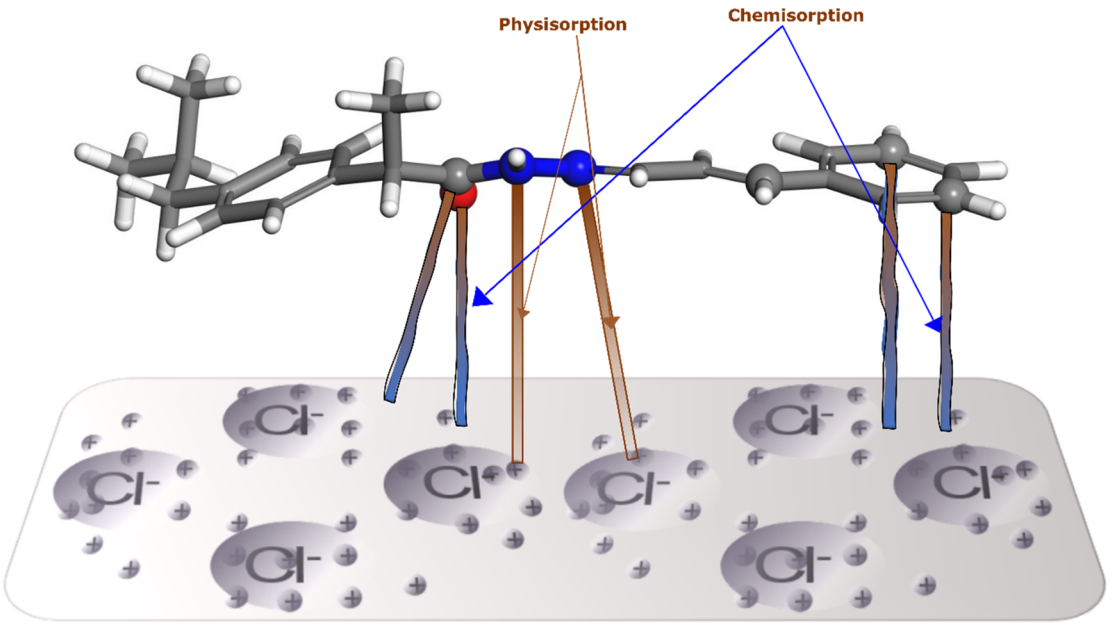

Figure 7. Schematic representation showing the potential interactions between inhibitors' active sites and the iron surface. The IPP molecule is selected as a reference example.

adsorption systems are needed to confirm the nature of inhibitor-Fe(110) interactions. The partial density of states is a valuable tool for investigating the binding and charge transfer characteristics between inhibitor molecules and the iron surface. The differences in chemical states between adsorbed and isolated inhibitor molecules can prove whether a charge transfer is absent or present.[56,57] The partial density of states (PDOSs) of isolated inhibitor molecules were determined after placing them far from the iron surface by 7 Å. PDOSs of adsorbed molecules are also determined after full DFB optimization, as represented in Figure 6. Fe 3d states are found inside the energy gap of the inhibitor molecules; thus, all states are limited to a −5/+5 energy range.[58]

A comparison between the chemical states of isolated (Figure 6a,b) and adsorbed (Figure 6c,d) inhibitor molecules reveals the presence of significant overlaps between the PDOSs of molecules atoms and iron atoms in the studied energy range. Therefore, strong charge transfer and hybridization are expected to occur upon the adsorption of molecules on the Fe(110) surface. The iron atoms' outer vacant *d* orbitals offer high possibilities for charge transfer. Interestingly, the PDOSs of adsorbed molecules (Figure 6c,d) show a high shift toward low energies compared to isolated molecules, which indicates a stable adsorption system.[59] Also, after the adsorption of inhibitor molecules on the iron surface, we notice a significant change in shape and intensity of peaks compared to isolated states, confirming that a strong electronic state hybridization occurs.[12] This is strong evidence for the dominant charge transfer between the inhibitors' active sites and vacant iron *d* orbitals.[12]

3.8. Corrosion Inhibition Mechanism. Corrosion inhibitors are now widely used to slow down the dissolution of the material. The inhibition process consists mainly of changing the surface termination of the metal and then creating a barrier against corrosion attack. However, despite the greater amount of literature dealing with corrosion inhibitors, a complete fundamental understanding of the corrosion inhibition process still has many gaps.[60] Therefore, it is of paramount importance to contribute to this effort, aiming to create a knowledge-based approach to developing effective corrosion inhibitors. In this work, newly synthesized hydrazones were found to be highly effective against acid corrosion in a highly concentrated HCl solution. First insights about the inhibition mechanism were obtained from EIS tests, which revealed that increasing inhibitor concentrations led to modifications of the double-layer behavior. It was found that increasing the amount of inhibitors increased the double layer thickness, which decreased the effective double-layer capacitance. It confirms that, like most organic inhibitors, present compounds exert the inhibition by adsorbing on the metal surface. Besides, *ab initio* modeling was employed to interpret and analyze the interactions between inhibitor molecules and the iron surface. We found that, in both cases, inhibitor molecules chemically coordinate with iron atoms through a charge transfer process that is confirmed by the strong hybridization of s and p states of inhibitor molecules. The atoms of the carbonyl group had a stronger affinity to the iron surface, whereas no covalent bonds were formed between nitrogen atoms and the iron surface. It is mainly attributed to long-range van der Waals interactions between N atoms and iron surface. In real conditions, such interactions are the first contact between inhibitor molecules and the iron surface.

It is well-known that inhibitor molecules get protonated in an acidic medium.[61] On the other hand, it has been widely reported that the steel surface is positively charged in HCl media.[62,63] The potential of zero charge (PZC) analysis conducted on many steel/inhibitor interfaces confirms the positive charge of steel surface in inhibited HCl mediums.[62−65] Thus, chloride ions will quickly adsorb on the positively charged metal surface, creating an excess negative charge and physically interacting with protonated inhibitor molecules.[66] When inhibitor molecules are close to the iron surface, chemical interactions can occur through charge transfer between the molecules' active sites and iron atoms' outer unfilled *d* orbitals. In addition, there is also a high chance for the retro-donation process from the metal to antibonding

https://doi.org/10.1021/acs.langmuir.2c02132
Langmuir 2022, 38, 15937−15949

orbitals of inhibitor molecules to reduce the excess charge on the metal.[38,67,68] A graphical representation of the proposed mechanism is shown in Figure 7.

4. CONCLUSIONS

In the present work, novel hydrazone compounds were synthesized by functionalizing the NSAID ibuprofen and applied for corrosion mitigation of N80 steel in a strong acidic medium (15 wt % HCl). A combined experimental and theoretical approach consisting of chemical, electrochemical, FE-SEM, and *ab initio* DFTB modeling was used to investigate the corrosion inhibition performance and interaction mechanism of tested compounds with the N80 steel surface. Electrochemical results indicated that both inhibitor molecules effectively adsorbed on the N80 steel surface by forming an inhibitor film, thus significantly lowering the effective double layer capacitance. Also, results showed that the investigated compounds had a strong inhibition effect on both anodic and cathodic corrosion reactions. The compounds under study exhibited a higher corrosion inhibition at very low concentrations; at 10^{-4} mol/L, the inhibition efficiency was 92% and 91%, then increased to 99% and 98% at 5×10^{-3} mol/L for CIP and IPP compounds, respectively. The adsorption of the investigated compounds followed the Langmuir isotherm model, while the calculated thermodynamic parameters supported the physicochemical nature of adsorption. FE-SEM and AFM analyses supported the high performance of the tested compounds, which was revealed from the significantly smoother surface morphology compared to the control test. DFTB simulation revealed that inhibitor molecules can create covalent and physical interactions with iron atoms, which was further confirmed by PDOSs analysis. The combined experimental and theoretical approaches used in the present study provided valuable insights into the interaction mechanisms and inhibition performance of selected compounds, which can be used as strong knowledge-based results for future explorations.

■ ASSOCIATED CONTENT

Supporting Information

The Supporting Information is available free of charge at https://pubs.acs.org/doi/10.1021/acs.langmuir.2c02132.

Full synthesis details; quantum chemical parameters details; weight loss data; electrical equivalent circuit; Nyquist EIS curves of N80 steel in 15 wt % HCl inhibited with 5×10^{-3} mol/L IPP at varied times; Langmuir isotherm plots for N80 steel in 15 wt % HCl containing different concentrations of IPP and CIP inhibitors at 303 K; comparison of the inhibition efficiency of tested hydrazones with other corrosion inhibitors for steels in 15 wt % HCl; thermodynamic parameters for the adsorption of IPP and ICP on N80 steel surface in 15 wt % HCl at 303 K; global reactivity descriptors; molecular dynamics simulation (PDF)

■ AUTHOR INFORMATION

Corresponding Authors

Hassane Lgaz − *Innovative Durable Building and Infrastructure Research Center, Center for Creative Convergence Education, Hanyang University ERICA, Ansan-si, Gyeonggi-do 15588, Korea;* orcid.org/0000-0001-8506-5759; Email: hlgaz@hanyang.ac.kr

Han-Seung Lee − *Department of Architectural Engineering, Hanyang University-ERICA, Sangrok-gu, Ansan 15588, Korea*; Email: ercleehs@hanyang.ac.kr

Authors

Badr El-Haitout − *Laboratory of Applied Chemistry and Environment, ENSA, University Ibn Zohr, 1136 Agadir, Morocco*

Chaymae Hejjaj − *Materials Science, Energy and Nano-engineering Department, Mohammed VI Polytechnic University (UM6P), 43150 Benguerir, Morocco*

Mustafa R. Al-Hadeethi − *Department of Chemistry, College of Education, University of Kirkuk, Kirkuk 36001, Iraq*

Omeed Maroof Ali − *Department of Chemistry, College of Education, University of Kirkuk, Kirkuk 36001, Iraq*

Ismat H. Ali − *Department of Chemistry, College of Science, King Khalid University, 61413 Abha, Saudi Arabia*

Rachid Salghi − *Laboratory of Applied Chemistry and Environment, ENSA, University Ibn Zohr, 1136 Agadir, Morocco*

Complete contact information is available at: https://pubs.acs.org/10.1021/acs.langmuir.2c02132

Notes

The authors declare no competing financial interest.

■ ACKNOWLEDGMENTS

This work was supported by the National Research Foundation of Korea (NRF) grant funded by the Korea government (MSIT) (No. NRF-2018R1A5A1025137). The authors extend their appreciation to the Deanship of Scientific Research at King Khalid University for funding this work through research groups program under grant number R.G.P.2/84/43.

■ REFERENCES

(1) Haruna, K.; Saleh, T. A. N,N′-Bis-(2-Aminoethyl)Piperazine Functionalized Graphene Oxide (NAEP-GO) as an Effective Green Corrosion Inhibitor for Simulated Acidizing Environment. *J. Environ. Chem. Eng.* **2021**, *9* (1), 104967.

(2) Thoume, A.; Left, D. B.; Elmakssoudi, A.; Achagar, R.; Dakir, M.; Azzi, M.; Zertoubi, M. Performance Evaluation of New Chalcone Oxime Functionalized Graphene Oxide as a Corrosion Inhibitor for Carbon Steel in a Hydrochloric Acid Solution. *Langmuir* **2022**, *38* (24), 7472−7483.

(3) Guo, L.; Zhu, M.; He, Z.; Zhang, R.; Kaya, S.; Lin, Y.; Saji, V. S. One-Pot Hydrothermal Synthesized Nitrogen and Sulfur Codoped Carbon Dots for Acid Corrosion Inhibition of Q235 Steel. *Langmuir* **2022**, *38* (13), 3984−3992.

(4) Ahmad, Z.*Principles of Corrosion Engineering and Corrosion Control*; Elsevier, 2006.

(5) Popov, B. N.*Corrosion Engineering: Principles and Solved Problems*; Elsevier, 2015.

(6) Zhao, F.; Wang, S.; Guo, J. Experimental and Molecular Dynamics Simulation Study on the Effects of the Carbon Chain Length of Gemini Surfactants on the Inhibition of the Acid-Rock Reaction Rate. *Langmuir* **2021**, *37* (17), 5232−5241.

(7) Quraishi, M. A.; Chauhan, D. S.; Saji, V. S.*Heterocyclic Organic Corrosion Inhibitors: Principles and Applications*; Elsevier, 2020.

(8) Verma, C.; Ebenso, E. E.; Bahadur, I.; Quraishi, M. A. An Overview on Plant Extracts as Environmental Sustainable and Green Corrosion Inhibitors for Metals and Alloys in Aggressive Corrosive Media. *J. Mol. Liq.* **2018**, *266*, 577−590.

(9) Hassan, R. M.; Ibrahim, S. M. Performance and Efficiency of Methyl-Cellulose Polysaccharide as a Green Promising Inhibitor for

Inhibition of Corrosion of Magnesium in Acidic Solutions. *J. Mol. Struct.* **2021**, *1246*, 131180.
(10) Du, T.; Chen, J.; Cao, D. N,N-Dipropynoxy Methyl Amine Trimethyl Phosphonate as Corrosion Inhibitor for Iron in Sulfuric Acid. *J. Mater. Sci.* **2001**, *36* (16), 3903−3907.
(11) Berrissoul, A.; Loukili, E.; Mechbal, N.; Benhiba, F.; Guenbour, A.; Dikici, B.; Zarrouk, A.; Dafali, A. Anticorrosion Effect of a Green Sustainable Inhibitor on Mild Steel in Hydrochloric Acid. *J. Colloid Interface Sci.* **2020**, *580*, 740−752.
(12) Lgaz, H.; Lee, H. Facile Preparation of New Hydrazone Compounds and Their Application for Long-Term Corrosion Inhibition of N80 Steel in 15% HCl: An Experimental Study Combined with DFTB Calculations. *J. Mol. Liq.* **2022**, *347*, 117952.
(13) Singh, A.; Ansari, K. R.; Quraishi, M. A.; Banerjee, P. Corrosion Inhibition and Adsorption of Imidazolium Based Ionic Liquid over P110 Steel Surface in 15% HCl under Static and Dynamic Conditions: Experimental, Surface and Theoretical Analysis. *J. Mol. Liq.* **2021**, *323*, 114608.
(14) Lgaz, H.; Salghi, R.; Masroor, S.; Kim, S.-H.; Kwon, C.; Kim, S. Y.; Yang, Y.-J.; Chung, I.-M. Assessing Corrosion Inhibition Characteristics of Hydrazone Derivatives on Mild Steel in HCl: Insights from Electronic-Scale DFT and Atomic-Scale Molecular Dynamics. *J. Mol. Liq.* **2020**, *308*, 112998.
(15) Lgaz, H.; Chung, I.-M.; Albayati, M. R.; Chaouiki, A.; Salghi, R.; Mohamed, S. K. Improved Corrosion Resistance of Mild Steel in Acidic Solution by Hydrazone Derivatives: An Experimental and Computational Study. *Arab. J. Chem.* **2020**, *13* (1), 2934−2954.
(16) Khamaysa, O. M. A.; Selatnia, I.; Lgaz, H.; Sid, A.; Lee, H.-S.; Zeghache, H.; Benahmed, M.; Ali, I. H.; Mosset, P. Hydrazone-Based Green Corrosion Inhibitors for API Grade Carbon Steel in HCl: Insights from Electrochemical, XPS, and Computational Studies. *Colloids Surf. -Physicochem. Eng. Asp.* **2021**, *626*, 127047.
(17) Lesko, S. M.; Mitchell, A. A. An Assessment of the Safety of Pediatric Ibuprofen: A Practitioner-Based Randomized Clinical Trial. *JAMA* **1995**, *273* (12), 929−933.
(18) Rollas, S.; Küçükgüzel, S. G. Biological Activities of Hydrazone Derivatives. *Molecules* **2007**, *12* (8), 1910−1939.
(19) Kokalj, A. Corrosion Inhibitors: Physisorbed or Chemisorbed? *Corros. Sci.* **2022**, *196*, 109939.
(20) Obot, I. B.; Haruna, K.; Saleh, T. A. Atomistic Simulation: A Unique and Powerful Computational Tool for Corrosion Inhibition Research. *Arab. J. Sci. Eng.* **2019**, *44* (1), 1−32.
(21) Guo, L.; Qi, C.; Zheng, X.; Zhang, R.; Shen, X.; Kaya, S. Toward Understanding the Adsorption Mechanism of Large Size Organic Corrosion Inhibitors on an Fe(110) Surface Using the DFTB Method. *RSC Adv.* **2017**, *7* (46), 29042−29050.
(22) Guo, L.; Wu, M.; Kaya, S.; Chen, M.; Madkour, L. H. Influence of the Alkyl Chain Length of Alkyltriazoles on the Corrosion Inhibition of Iron: A DFTB Study. *AIP Conf. Proc.* **2018**, *1995* (1), 020015.
(23) Kokalj, A.; Peljhan, S.; Finšgar, M.; Milošev, I. What Determines the Inhibition Effectiveness of ATA, BTAH, and BTAOH Corrosion Inhibitors on Copper? *J. Am. Chem. Soc.* **2010**, *132* (46), 16657−16668.
(24) Kokalj, A. Is the Analysis of Molecular Electronic Structure of Corrosion Inhibitors Sufficient to Predict the Trend of Their Inhibition Performance. *Electrochim. Acta* **2010**, *56* (2), 745−755.
(25) Kokalj, A. Ab Initio Modeling of the Bonding of Benzotriazole Corrosion Inhibitor to Reduced and Oxidized Copper Surfaces. *Faraday Discuss.* **2015**, *180* (0), 415−438.
(26) Kokalj, A.; Lozinšek, M.; Kapun, B.; Taheri, P.; Neupane, S.; Losada-Pérez, P.; Xie, C.; Stavber, S.; Crespo, D.; Renner, F. U.; Mol, A.; Milošev, I. Simplistic Correlations between Molecular Electronic Properties and Inhibition Efficiencies: Do They Really Exist? *Corros. Sci.* **2021**, *179*, 108856.
(27) Kokalj, A.; Behzadi, H.; Farahati, R. DFT Study of Aqueous-Phase Adsorption of Cysteine and Penicillamine on Fe(110): Role of Bond-Breaking upon Adsorption. *Appl. Surf. Sci.* **2020**, *514*, 145896.
(28) El-Haitout, B.; Selatnia, I.; Lgaz, H.; Al-Hadeethi, M. R.; Lee, H.-S.; Chaouiki, A.; Ko, Y. G.; Ali, I. H.; Salghi, R. Exploring the Feasibility of New Eco-Friendly Heterocyclic Compounds for Establishing Efficient Corrosion Protection for N80 Steel in a Simulated Oil Well Acidizing Environment: From Molecular-Level Prediction to Experimental Validation. *Colloids Surf. Physicochem. Eng. Asp.* **2023**, *656*, 130372.
(29) Scully, J.; Baboian, R.*Standard Practice for Laboratory Immersion Corrosion Testing of Metals*; ASTM: Philadelphia, PA, 1995; pp 110.
(30) Perdew, J. P.; Burke, K.; Ernzerhof, M. Generalized Gradient Approximation Made Simple. *Phys. Rev. Lett.* **1996**, *77* (18), 3865.
(31) Klamt, A.; Schüürmann, G. COSMO: A New Approach to Dielectric Screening in Solvents with Explicit Expressions for the Screening Energy and Its Gradient. *J. Chem. Soc. Perkin Trans. 2* **1993**, No. 5, 799−805.
(32) Hourahine, B.; Aradi, B.; Blum, V.; Bonafé, F.; Buccheri, A.; Camacho, C.; Cevallos, C.; Deshaye, M.; Dumitrică, T.; Dominguez, A.; et al. DFTB+, a Software Package for Efficient Approximate Density Functional Theory Based Atomistic Simulations. *J. Chem. Phys.* **2020**, *152* (12), 124101.
(33) Mayo, S. L.; Olafson, B. D.; Goddard, W. A. DREIDING: A Generic Force Field for Molecular Simulations. *J. Phys. Chem.* **1990**, *94* (26), 8897−8909.
(34) Kertit, S.; Chaouket, F.; Srhiri, A.; Keddam, M. Corrosion Inhibition of Amorphous FeBSiC Alloy in 1 m HCl by 3-Amino-1,2,4-Triazole. *J. Appl. Electrochem.* **1994**, *24* (11), 1139−1145.
(35) Thanapackiam, P.; Rameshkumar, S.; Subramanian, S. S.; Mallaiya, K. Electrochemical Evaluation of Inhibition Efficiency of Ciprofloxacin on the Corrosion of Copper in Acid Media. *Mater. Chem. Phys.* **2016**, *174*, 129−137.
(36) Shainy, K. M.; Rugmini Ammal, P.; Unni, K. N.; Benjamin, S.; Joseph, A. Surface Interaction and Corrosion Inhibition of Mild Steel in Hydrochloric Acid Using Pyoverdine, an Eco-Friendly Bio-Molecule. *J. Bio- Tribo-Corros.* **2016**, *2* (3), 20.
(37) Migahed, M. A.; Al-Sabagh, A. M.; Khamis, E. A.; Zaki, E. G. Quantum Chemical Calculations, Synthesis and Corrosion Inhibition Efficiency of Ethoxylated-[2-(2-{2-[2-(2-Benzenesulfonylamino-Ethylamino)-Ethylamino]-Ethylamino}-Ethylamino)-Ethyl]-4-Alkyl-Benzenesulfonamide on API X65 Steel Surface under H2S Environment. *J. Mol. Liq.* **2015**, *212*, 360−371.
(38) Singh, A.; Ansari, K. R.; Chauhan, D. S.; Quraishi, M. A.; Lgaz, H.; Chung, I.-M. Comprehensive Investigation of Steel Corrosion Inhibition at Macro/Micro Level by Ecofriendly Green Corrosion Inhibitor in 15% HCl Medium. *J. Colloid Interface Sci.* **2020**, *560*, 225−236.
(39) Orazem, M. E.; Tribollet, B.*Electrochemical Impedance Spectroscopy*; Wiley, 2008; pp 383−389.
(40) Liao, H.; Watson, W.; Dizon, A.; Tribollet, B.; Vivier, V.; Orazem, M. E. Physical Properties Obtained from Measurement Model Analysis of Impedance Measurements. *Electrochim. Acta* **2020**, *354*, 136747.
(41) Sadeghi Erami, R.; Amirnasr, M.; Meghdadi, S.; Talebian, M.; Farrokhpour, H.; Raeissi, K. Carboxamide Derivatives as New Corrosion Inhibitors for Mild Steel Protection in Hydrochloric Acid Solution. *Corros. Sci.* **2019**, *151*, 190−197.
(42) Laschuk, N. O.; Easton, E. B.; Zenkina, O. V. Reducing the Resistance for the Use of Electrochemical Impedance Spectroscopy Analysis in Materials Chemistry. *RSC Adv.* **2021**, *11* (45), 27925−27936.
(43) Mahdavian, M.; Attar, M. M. Another Approach in Analysis of Paint Coatings with EIS Measurement: Phase Angle at High Frequencies. *Corros. Sci.* **2006**, *48* (12), 4152−4157.
(44) Mahdavian A., M.; Attar, M.M. Investigation on Zinc Phosphate Effectiveness at Different Pigment Volume Concentrations via Electrochemical Impedance Spectroscopy. *Electrochim. Acta* **2005**, *50* (24), 4645−4648.
(45) Brug, G. J.; van den Eeden, A. L.; Sluyters-Rehbach, M.; Sluyters, J. H. The Analysis of Electrode Impedances Complicated by

https://doi.org/10.1021/acs.langmuir.2c02132
Langmuir 2022, 38, 15937−15949

the Presence of a Constant Phase Element. *J. Electroanal. Chem. Interfacial Electrochem.* **1984**, *176* (1−2), 275−295.
(46) Shahryari, Z.; Gheisari, K.; Yeganeh, M.; Ramezanzadeh, B. Corrosion Mitigation Ability of Differently Synthesized Polypyrrole (PPy-FeCl3 & PPy-APS) Conductive Polymers Modified with Na2MoO4 on Mild Steel in 3.5% NaCl Solution: Comparative Study and Optimization. *Corros. Sci.* **2021**, *193*, 109894.
(47) Al-Refaie, A. A.; Walton, J.; Cottis, R. A.; Lindsay, R. Photoelectron Spectroscopy Study of the Inhibition of Mild Steel Corrosion by Molybdate and Nitrite Anions. *Corros. Sci.* **2010**, *52* (2), 422−428.
(48) Hirschorn, B.; Orazem, M. E.; Tribollet, B.; Vivier, V.; Frateur, I.; Musiani, M. Determination of Effective Capacitance and Film Thickness from Constant-Phase-Element Parameters. *Electrochim. Acta* **2010**, *55* (21), 6218−6227.
(49) Guo, L.; Bakri, Y. E.; Yu, R.; Tan, J.; Essassi, E. M. Newly Synthesized Triazolopyrimidine Derivative as an Inhibitor for Mild Steel Corrosion in HCl Medium: An Experimental and in Silico Study. *J. Mater. Res. Technol.* **2020**, *9* (3), 6568−6578.
(50) Boulhaoua, M.; El Hafi, M.; Zehra, S.; Eddaif, L.; Alrashdi, A. A.; Lahmidi, S.; Guo, L.; Mague, J. T.; Lgaz, H. Synthesis, Structural Analysis and Corrosion Inhibition Application of a New Indazole Derivative on Mild Steel Surface in Acidic Media Complemented with DFT and MD Studies. *Colloids Surf. Physicochem. Eng. Asp.* **2021**, *617*, 126373.
(51) Guo, L.; Kaya, S.; Obot, I. B.; Zheng, X.; Qiang, Y. Toward Understanding the Anticorrosive Mechanism of Some Thiourea Derivatives for Carbon Steel Corrosion: A Combined DFT and Molecular Dynamics Investigation. *J. Colloid Interface Sci.* **2017**, *506*, 478−485.
(52) Dutta, A.; Saha, S. Kr.; Banerjee, P.; Sukul, D. Correlating Electronic Structure with Corrosion Inhibition Potentiality of Some Bis-Benzimidazole Derivatives for Mild Steel in Hydrochloric Acid: Combined Experimental and Theoretical Studies. *Corros. Sci.* **2015**, *98*, 541−550.
(53) Saha, S. K.; Dutta, A.; Ghosh, P.; Sukul, D.; Banerjee, P. Novel Schiff-Base Molecules as Efficient Corrosion Inhibitors for Mild Steel Surface in 1 M HCl Medium: Experimental and Theoretical Approach. *Phys. Chem. Chem. Phys.* **2016**, *18* (27), 17898−17911.
(54) Obot, I. B.; Macdonald, D. D.; Gasem, Z. M. Density Functional Theory (DFT) as a Powerful Tool for Designing New Organic Corrosion Inhibitors. Part 1: An Overview. *Corros. Sci.* **2015**, *99*, 1−30.
(55) Cordero, B.; Gomez, V.; Platero-Prats, A. E.; Reves, M.; Echeverria, J.; Cremades, E.; Barragan, F.; Alvarez, S. Covalent Radii Revisited. *Dalton Trans.* **2008**, *0* (21), 2832−2838.
(56) Kumar, D.; Jain, V.; Rai, B. Unravelling the Mechanisms of Corrosion Inhibition of Iron by Henna Extract: A Density Functional Theory Study. *Corros. Sci.* **2018**, *142*, 102−109.
(57) Murmu, M.; Saha, S. Kr.; Murmu, N. C.; Banerjee, P. Effect of Stereochemical Conformation into the Corrosion Inhibitive Behaviour of Double Azomethine Based Schiff Bases on Mild Steel Surface in 1 Mol L-1 HCl Medium: An Experimental, Density Functional Theory and Molecular Dynamics Simulation Study. *Corros. Sci.* **2019**, *146*, 134−151.
(58) Özcan, M.; Toffoli, D.; Üstünel, H.; Dehri, İ. Insights into Surface-Adsorbate Interactions in Corrosion Inhibition Processes at the Molecular Level. *Corros. Sci.* **2014**, *80*, 482−486.
(59) Yalet, N. M.; Ranea, V. A. A DFT+U Study on the Adsorption of CO, H2S, PH3, CO2 and SO2 on the V2O5(001) Surface with Atomic Rh Adsorbed. *Surf. Sci.* **2022**, *718*, 122014.
(60) Kousar, K.; Dowhyj, M.; Walczak, M. S.; Ljungdahl, T.; Wetzel, A.; Oskarsson, H.; Walton, A. S.; Restuccia, P.; Harrison, N. M.; Lindsay, R. Corrosion Inhibition in Acidic Environments: Key Interfacial Insights with Photoelectron Spectroscopy. *Faraday Discuss.* **2022**, *236*, 374.
(61) Solmaz, R. Investigation of Adsorption and Corrosion Inhibition of Mild Steel in Hydrochloric Acid Solution by 5-(4-Dimethylaminobenzylidene)Rhodanine. *Corros. Sci.* **2014**, *79*, 169−176.
(62) Deng, S.; Li, X.; Fu, H. Acid Violet 6B as a Novel Corrosion Inhibitor for Cold Rolled Steel in Hydrochloric Acid Solution. *Corros. Sci.* **2011**, *53* (2), 760−768.
(63) Mobin, M.; Basik, M.; Aslam, J. Pineapple Stem Extract (Bromelain) as an Environmental Friendly Novel Corrosion Inhibitor for Low Carbon Steel in 1 M HCl. *Measurement* **2019**, *134*, 595−605.
(64) Aslam, J.; Aslam, R.; Alrefaee, S. H.; Mobin, M.; Aslam, A.; Parveen, M.; Mustansar Hussain, C. Gravimetric, Electrochemical, and Morphological Studies of an Isoxazole Derivative as Corrosion Inhibitor for Mild Steel in 1M HCl. *Arab. J. Chem.* **2020**, *13* (11), 7744−7758.
(65) Qiang, Y.; Zhang, S.; Tan, B.; Chen, S. Evaluation of Ginkgo Leaf Extract as an Eco-Friendly Corrosion Inhibitor of X70 Steel in HCl Solution. *Corros. Sci.* **2018**, *133*, 6−16.
(66) Solmaz, R.; Altunbaş, E.; Kardaş, G. Adsorption and Corrosion Inhibition Effect of 2-((5-Mercapto-1,3,4-Thiadiazol-2-Ylimino)-Methyl)Phenol Schiff Base on Mild Steel. *Mater. Chem. Phys.* **2011**, *125* (3), 796−801.
(67) Chaouiki, A.; Lgaz, H.; Zehra, S.; Salghi, R.; Chung, I.-M.; El Aoufir, Y.; Bhat, K. S.; Ali, I. H.; Gaonkar, S. L.; Khan, M. I.; Oudda, H. Exploring Deep Insights into the Interaction Mechanism of a Quinazoline Derivative with Mild Steel in HCl: Electrochemical, DFT, and Molecular Dynamic Simulation Studies. *J. Adhes. Sci. Technol.* **2019**, *33* (9), 921−944.
(68) Chugh, B.; Singh, A. K.; Thakur, S.; Pani, B.; Pandey, A. K.; Lgaz, H.; Chung, I.-M.; Ebenso, E. E. An Exploration about the Interaction of Mild Steel with Hydrochloric Acid in the Presence of N-(Benzo[d]Thiazole-2-Yl)-1-Phenylethan-1-Imines. *J. Phys. Chem. C* **2019**, *123* (37), 22897−22917.

https://doi.org/10.1021/acs.langmuir.2c02132
Langmuir 2022, 38, 15937−15949